Fabrication of a NCD microelectrode array for amperometric detection with micrometer spatial resolution

Diamond & Related Materials 20 (2011) 793–797

Contents lists available at ScienceDirect

Diamond & Related Materials

journal homepage: www.elsevier.com/locate/diamond

Fabrication of a NCD microelectrode array for amperometric detection with micrometer spatial resolution☆☆

E. Colombo [a,b,*], Y. Men [a], J. Scharpf [a], C. Pietzka [a], M. Dipalo [a], P. Herfurth [a], Z. Gao [a], M. Schneider [c], V. Carabelli [b], E. Carbone [b], E. Kohn [a], A. Pasquarelli [a]

[a] Institute of Electron Devices and Circuits, University of Ulm, Germany
[b] Department of Neuroscience and Nanostructured Interfaces and Surfaces Excellence Center, University of Torino, Italy
[c] Experimental Anaesthesiology Section, Department of Clinical Anaesthesiology, Ulm University Hospital, Germany

ARTICLE INFO

Available online 5 April 2011

Keywords:
NCD
MEA
Micrometric spatial resolution
Transparency

ABSTRACT

We report on the fabrication of a boron-doped nanocrystalline diamond (NCD) 3×3 high-density microelectrode array (MEA) for amperometric measurements, with a single electrode area of 3×5 μm^2 and a separation in the μm scale. The NCD microelectrodes were grown by hot filament chemical vapor deposition (HFCVD) on a double-side polished sapphire wafer in order to preserve the diamond transparency. Bias enhanced nucleation (BEN) was performed to ensure a covalent adhesion of the films to the substrate. A current background noise of less than 5 pA peak to peak over a 1 kHz bandwidth resulted from an electrochemical investigation of the new device, using 100 mM KCl solutions and ferrocyanide red-ox couples. Cyclic voltammetry measurements in physiological buffer solution and in the presence of oxidizable bio-molecules strengthened its suitability for bio-sensing. When compared to a 2×2 NCD microelectrode array prototype, already used for *in vitro* cell measurements, the signal to noise ratio of the amperometric response of the new 3×3 device proved twice as good. In addition, the optical transmittance of the boron-doped thin layers exceeded 40% in the visible wavelength range.
The excellent electrochemical properties of NCD electrodes and the transparency in combination with the high spatial resolution make the new 3×3 NCD MEA a promising tool for electrochemical sensing in a variety of applications, ranging from medical to industrial, in neutral or harsh environments.

1. Introduction

NCD electrodes have been recognized as a promising tool for electrochemical sensing due to their extraordinary electrochemical performances: a very low background current (<1 μA/cm^2), a water dissociation potential window around 3 V, a high biocompatibility and an outstanding inertness in harsh environment [1,2]. Electroanalysis of substances like phenol or bio-molecules like glutathione are typically outside the usable potential window of standard electrodes such as carbon fibers or noble metals (Au, Pt), but these analytes have been detected with NCD electrodes [3,4]. Moreover, diamond surfaces can easily be functionalized [5–8] and are highly inert in electrolyte. Harsh environment applications have been extensively studied and the high corrosion stability of NCD electrodes was confirmed [2,9]. Additionally, diamond can be either insulating or quasi-metallic and has an extended range of transparency (225 nm–12 μm) [10] due to its wide bandgap semiconductor characteristics. NCD microelectrode and ultra-micro-electrode arrays have been also widely studied and used in the fields of electro-analysis and life science [11–14].

To date, NCD technology was mainly developed on silicon (Si), the fundamental material for modern integration microelectronics. However, Si substrates transmit only infrared light of wavelengths above 1.1 μm, which restricts the range of possible optical applications. Biochemical and neurophysiologic preparations, for instance, commonly use UV–visible transmission microscopy and fluorescence analysis. Transparent devices, however, can be produced in diamond technology thanks to the last decades' efforts in growing diamond on transparent substrates, like glass, quartz or even high-temperature-stable plastic [15–17]. It was even possible to combine diamond with CMOS (Complementary Metal Oxide Semiconductor) technologies on sapphire whereby a tolerable transparency could be preserved [18]. More recently, the first prototypes of NCD microelectrode arrays on transparent substrate were fabricated [19] and we lately reported on a first 2×2 microelectrode array out of boron-doped NCD on sapphire [20]. The latter NCD microelectrode array was successfully employed *in vitro* with living cells, resolving with high time resolution bursts of amperometric spikes associated to the quantal release of adrenaline from mouse chromaffin cells [21], achieving a first spatially resolved

☆☆ Presented at the Diamond 2010, 21st European Conference on Diamond, Diamond- Like Materials, Carbon Nanotubes, and Nitrides, Budapest.

* Corresponding author at: Institute of Electron Devices and Circuits, University of Ulm, Germany.
E-mail address: elisabetta.colombo@uni-ulm.de (E. Colombo).

0925-9635/$ – see front matter © 2011 Elsevier B.V. All rights reserved.
doi:10.1016/j.diamond.2011.03.032

detection of those signals [22]. We have demonstrated also that this 2×2 microelectrode array shows the same red-ox sensitivity during *in vitro* experiments as common carbon fiber microelectrodes [23].

Another trend is the miniaturization of devices for electrochemical sensing to obtain high spatial and temporal resolution with enhanced sensitivity, which inevitably creates the need for integrated read-out electronics following in the footsteps of silicon technology. An example of the trend towards high-density devices with integrated read-out electronics can be found in electrophysiological analysis [24], where microelectrode arrays are indeed a major tool since decades [25]. Here the interest in more detailed studies on generation and propagation of neuronal signals down to sub-cellular level or on specific cell membrane processes leads to the need of devices with a higher spatial resolution. Recently, there have been efforts to meet this demand using Si-based technologies, as for example high density CMOS microelectrode arrays [24,26] or 3D MEAs for intracellular recordings with even sub-cellular resolution [27,28], but the presence of a Si substrate makes these devices unsuitable for inverted microscopy, fluorescence recordings or other optical applications.

There is considerable interest in the integration of read-out electronics and NCD on a transparent substrate [18]. We have recently reported on the monolithic fabrication of GaN-based ion-sensitive field effect transistors (ISFETs) with boron-doped NCD gate electrodes working in amperometric and potentiometric modes [29]. The GaN devices and NCD layers are both grown on sapphire substrate, which ensures full exploitation of the intrinsic transparency of the semiconductor.

We present here the first transparent nanocrystalline diamond high-density microelectrode array for electrochemical sensing with micrometer spatial resolution. A 3×3 array of boron-doped NCD microelectrodes was patterned on a double-side polished sapphire substrate with a separation distance between electrodes in the μm range and extending over 480 μm^2 approximately. Each microelectrode of the array can be addressed separately. The device had been designed earlier to host GaN-based FETs and their interconnections. Characterization and early tests in electrolytes and in the presence of red-ox couples were realized. The comparison of the cyclic voltammograms of the new 3×3 microelectrode array with the previous 2×2 prototype showed an improved current density of bio-molecule oxidation. Optical spectroscopy measurements demonstrated the preserved transparency of the new device.

2. Experimental

A double side polished sapphire wafer (Epistone, 2″ DSP wafers) was used as substrate material for the diamond growth. The NCD film was deposited by means of HFCVD and a bias-enhanced nucleation (BEN) process was chosen to insure strong covalent adhesion of the NCD films to the substrate. Due to the need of a conductive substrate to perform BEN, thin conductive interlayers were deposited on the sapphire to be used as a nucleation layer for the growth of the undoped NCD buffer layer; the interlayers materials and thicknesses were tuned in order to minimize light absorption and to maximize the nucleation density [30]. This process led to a nucleation density of approximately 3×10^{10} cm^{-2}, comparable with nucleation densities on standard Si wafers [31]. The BEN process was carried out with the following parameters: substrate temperature 800 °C, CH_4 to H_2 ratio 0.75%, pressure of 1.5 kPa. A 200 nm NCD intrinsic layer growth followed in the same HFCVD system with a substrate temperature of ~740 °C, a CH_4 to H_2 ratio of 0.3% and a pressure of 2.5 kPa. Homogeneous nucleation and growth were both performed on a quarter 2″ DSP sapphire wafer.

The resulting NCD intrinsic film was then patterned with the nine microelectrodes structure using e-beam lithography and reactive ion etching (RIE) in argon/oxygen plasma. This etching process was performed down to the sapphire substrate in order to insure the electrical insulation between the microelectrodes (>200 GΩ).

The structure was then overgrown by a ~250 nm boron doped NCD layer deposited by microwave plasma CVD at a power level of 700 W and a CH_4 to H_2 ratio of 0.6%. The substrate temperature was 750 °C and the process pressure 0.13 kPa. Boron doping was obtained using a solid boron rod inserted in the plasma [32].

The boron-doped NCD surface was chemically treated with chromosulphuric acid in order to remove possible graphitic content and to achieve an oxygen surface termination. Ohmic contacts were realized by optical lithography and Ti/Au deposition. A Si_xN_y passivation layer of approximately 1 μm thickness was deposited by plasma enhanced CVD and patterned by optical lithography and reactive ion etching.

Au bond-wires were used for the connections between the ohmic contacts and the measurement board. A glass ring was glued (Elastosil E43 transparent, silicone rubber) to the device to produce a ~100 μl chamber for the electrolyte. The finished chips were tested by electrochemical capacitance-voltage, cyclic voltammetry and amperometric measurements using either a potentiostat equipped with a reference saturated calomel electrode (SCE) and a Pt counter electrode or a new homemade portable two electrodes set-up, which makes use of an Ag/AgCl reference/counter electrode. The new portable system was developed to acquire the signals from the nine channels simultaneously and independently.

3. Results and discussion

The SEM micrograph of Fig. 1 shows the as-grown boron doped NCD surface with an average grain size ~100 nm. As shown in Fig. 2a, the boron doped NCD growth was tuned both in the vertical and horizontal directions leading to a complete covering of the conductive nucleation interlayers, which would have been otherwise exposed to electrolytes due to the diamond etching process down to the sapphire; Fig. 2b sketches the section view of such an overgrown structure.

The miniaturized design of the 3×3 microelectrode array is shown in Fig. 3a and b: a nominal 22×22 μm^2 square hole was opened in the passivation layer in correspondence with the center of the 3×3 array. Such Si_xN_y opening defines the active area of each microelectrode of the array to be 3×5 μm^2. The finished and packaged device is depicted in Fig. 3c.

Electrochemical capacitance-voltage measurements in 100 mM KCl solution, realized with the potentiostat, revealed a boron doping concentration of approximately 3×10^{20} cm^{-3}. In addition, to confirm the expected performances of the present device for electrochemical sensing, we chose a saline buffer solution which supports also the possibility to use the new device in biochemical applications: the 3×3 MEA were tested in Tyrode solution (5 mM KCl, 10 mM $CaCl_2$, pH = 7.4), the common buffer solution used during electrophysiological recordings

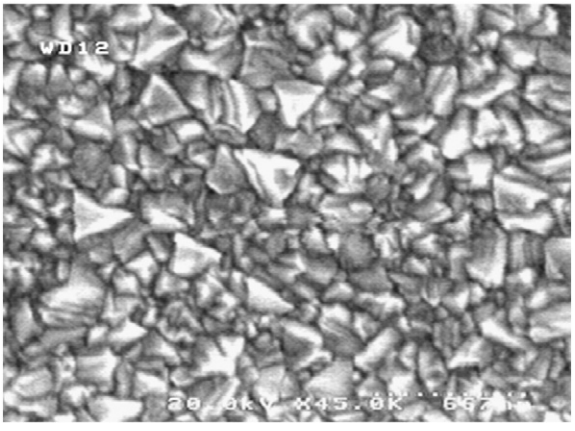

Fig. 1. SEM micrograph of the B-doped NCD surface.

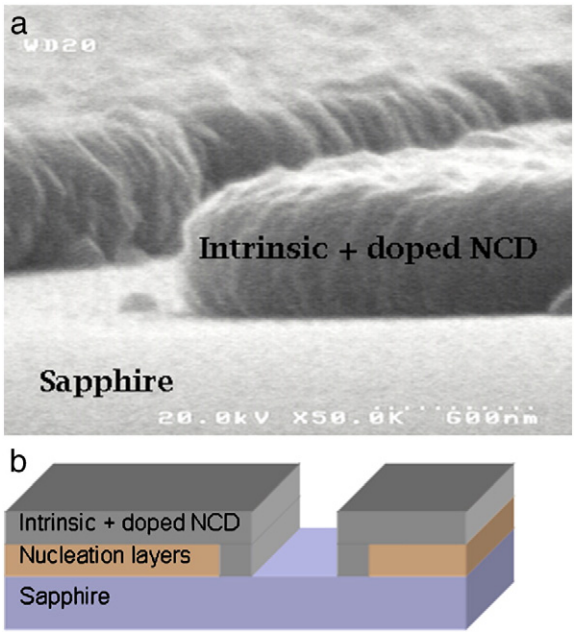

Fig. 2. a) SEM micrograph of the NCD microelectrodes: the side view shows the full covering of the microelectrodes due the B-doped NCD overgrowth made after the patterning of the NCD intrinsic film; b) schematic view of the structures depicted in panel a.

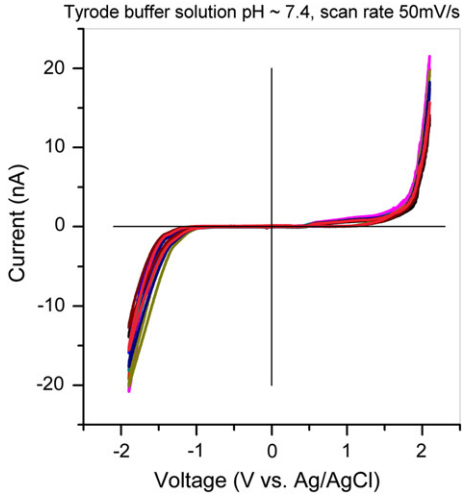

Fig. 4. The cyclic voltammograms recorded from the nine microelectrodes of the 3×3 array: the measurements were realized with a new portable nine channels set-up with respect to a Ag/AgCl reference/counter electrode at a scan-rate of 50 mV/s.

[21]. The 3×3 MEA, mounted on the new portable set-up, displayed in Tyrode buffer the typical 3 V water dissociation window of diamond and its low background currents (below 10 μA/cm^2; Fig. 4). A background noise of 5 pA peak to peak over a 1 kHz bandwidth was reached. Additionally, the nine microelectrodes showed similar cyclic voltammograms, the apparent differences being attributable to the minor variations of each active surface area.

An advantage of reducing the size of microelectrodes in a MEA is the improved signal to noise ratio, which is due to the low capacitive currents of the microelectrode or its enhanced mass transport caused by a dominant radial diffusion behavior. In the case of a macroelectrode, the oxidation (or reduction) current is limited by planar diffusion and typically shows a current peak in cyclic voltammetry measurements, where the peak current density depends on the scan rate: $j_{peak} \propto \sqrt{scan\,rate}$ [33]. On the other hand, the current density for a microelectrode is in the ideal case scan rate independent and shows a current plateau instead of a peak. A good approximation for our device could be a spherical-shaped microelectrode with radius r_0. In this case, the current density is expressed by [33,34]:

$$j = \frac{n\,F\,D c_0}{r_0} \tag{1}$$

where n is the number of exchanged electrons within the chemical reaction, F and D are respectively the Faraday and the diffusion constants and c_0 is the concentration of the red-ox species. Eq. (1) shows that the smaller electrode dimensions result in higher signal current densities. Such microelectrode characteristics could be indeed obtained with the present 3×3 array as show in Fig. 5a and b. These measurements were carried out with $Fe(CN)_6^{4-/3-}$ and adrenaline (Sigma-Aldrich), a key molecule in the processes of neurosecretion. The cyclic voltammograms of the microelectrodes in 100 mM KCl + 1 mM $Fe(CN)_6^{4-/3-}$ and in 100 mM KCl + 15 μM adrenaline (Fig. 5a and b, respectively) show the steady-state voltammograms shape and its typical plateau starting in correspondence of the oxidation voltage of the red-ox species. Fig. 5a and b depicts the representative results of the two experiments respectively from one of the nine microelectrodes, the response being uniform over the whole array. Since the measurements were performed in homogeneous electrolyte and the dilution of red-ox molecules occurred over a timescale of minutes, the

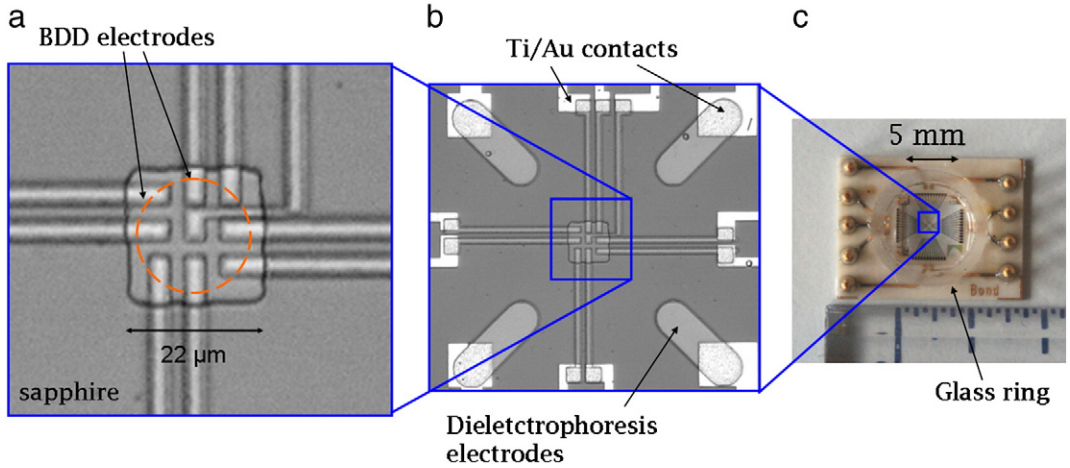

Fig. 3. a) Reflection optical microscopy image showing the center of the 3×3 NCD high density MEA with its 22×22 μm^2 active area. The dashed circle indicates the size of a neurosecretory cell. b) A larger view of the device which includes the ohmic contacts. c) The 3×3 NCD high density MEA packaged on the acquisition board and with the glass ring delimiting the perfusion chamber and the nine Au pins for electrical connections.

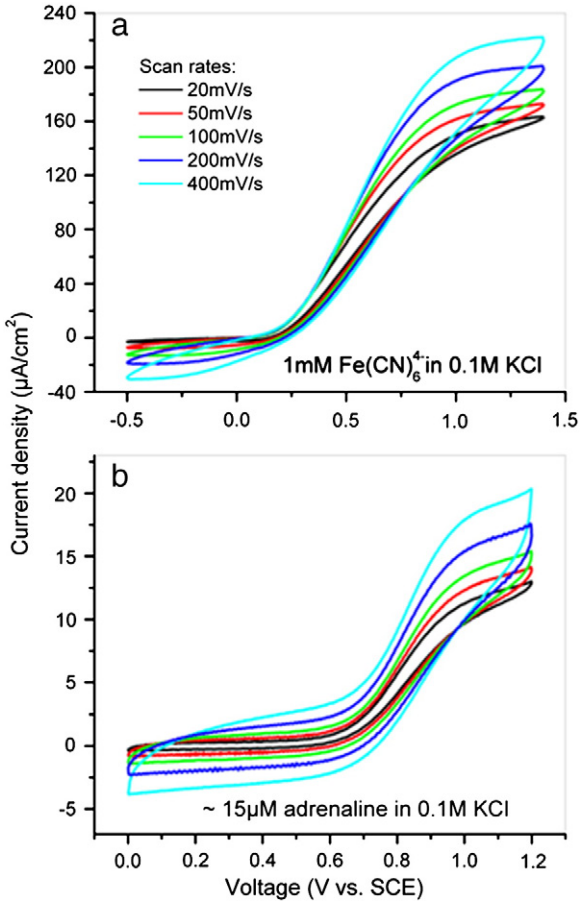

Fig. 5. Steady-state voltammograms recorded with the potentiostat in a)100 mM KCl + 1 mM $Fe(CN)_6^{4-/3-}$ and in b) 100 mM KCl + 15 μM adrenaline at scan rates varying from 20 to 400 mV/s.

registered amperometric signal is affected by the typical radial diffusion behavior of a microelectrode discussed above. We measured oxidation current densities variations of a factor 1.4 and 1.6 respectively for the experiments with ferrocyanide and adrenaline, when the scan rate was varied between 20 and 400 mV/s. A slight deviation from the ideal scan-rate independent behavior of microelectrodes was therefore observed. Nevertheless, the red-ox current density variations are small if compared with the theoretical factor expected for a large-scale electrode: for the same 20-fold scan-rate range, we would in fact detect a variation of $\sqrt{20} \approx 4.5$, which is almost 3 times higher than for our present 3×3 array. Moreover, we can appreciate in Fig. 5b a good correlation between the expected and measured maximum values of the oxidation current densities. The current density j obtained from Eq. (1) for the oxidation of adrenaline is approximately 40 μA/cm^2, assuming D ~6 ·10^6 cm^2/s [35,36] and $r_0 = 4$ μm. This value fits reasonably our data, considering that the geometry of microelectrodes is not hemi-spherical and that a precise evaluation of the active area should consider the nanocrystalline morphology of the NCD surface. On the other hand, the limiting current density measured for ferrocyanide (Fig. 5a) is lower than the value we should expect from Eq. (1) assuming the same values of D and r_0 [37]. We attributed this result to a phenomenon of saturation due to the relatively high concentration of red-ox species. Further electrochemical investigations of the response to ferrocyanide with the 3×3 array will be soon available.

Interestingly, our new 3×3 MEA with micrometer separation improves the electrochemical response with respect to our previous 2×2 MEA prototype. A comparison between the oxidation plateaus of adrenaline (the same molecule already detected *in vitro* with living cells) monitored with a 2×2 MEA prototype like the one described in [20] and the new 3×3 MEA is shown in Fig. 6. The measure highlights a clear 2-fold increase in the current density in correspondence with the oxidation plateau, while the background current is preserved below 2 μA/cm^2. Moreover, the 2-fold increase fits with the value forecasted by Eq. (1) considering that the area of one electrode of the previous 2×2 device was slightly larger than 30 μm^2. The comparison confirms the improvement in the signal to noise ratio for an amperometric detection achieved by the 3×3 MEA with respect to the previous prototype, while increasing the number of microelectrodes covering the same surface area. These electrochemical investigations with red-ox not only prove the discussed microelectrode behavior, but strengthen also the suitability of the present device for electrochemical/electrophysiological characterizations.

The radial diffusion regime of red-ox species is however achieved with microelectrode arrays only when the single electrodes are sufficiently separated to avoid overlapping diffusion fronts [33,34]: this is especially important for many microelectrode arrays shown in literature, where the only improved signal to noise ratio but no spatial resolution is desired [38] and all the microelectrodes are therefore short-circuited. Additionally, a too small separation could result in the loss of the spatial information, if the interspacing is in the same range or below the diffusion length of the red-ox species. However, *in vitro* experiments like the ones performed on our previous 2×2 MEA prototype could already give preliminary detection of cell activity signals with spatial resolution thanks to the short timescale of the release events (~ms range). The fast dynamics of such an experiment insured in fact that diffusion played a minor role and therefore a spatially resolved characterization of discrete release zones was achieved [20,21]. For this particular application and for dynamically similar ones, the new 3×3 array could reach therefore micrometer spatial resolution thanks to its miniaturized geometry with the improved electrochemical performances discussed above.

Finally, the transparency of the NCD microelectrodes was characterized as shown in Fig. 7. Curve A refers to a boron-doped electrode (~ 270 nm intrinsic HFCVD NCD + 50 nm boron-doped Plasma NCD) prepared like the one used for the reported fabrication of the 3×3 MEA, in which the reduced transparency towards the low wavelength range is attributed mainly to the presence of the interlayers needed for the BEN process [20]. The inset shows the device, mounted on the portable system, through the electrolyte at the transmission inverted microscope, demonstrating the suitability of the device for instance for bio-sensing. On the other hand, curve B in Fig. 7 illustrates early results on a boron-doped NCD film (~200 nm intrinsic NCD + 300 nm boron-doped NCD), also grown by HFCVD and

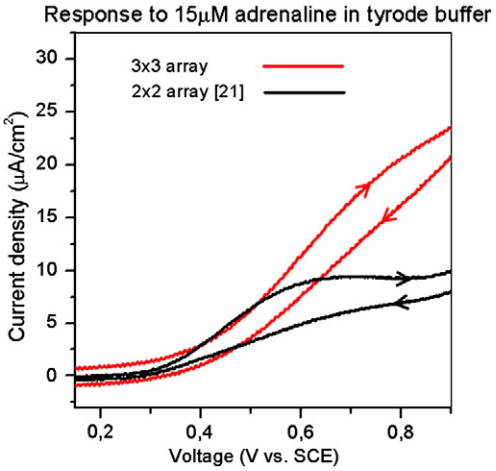

Fig. 6. Comparison between the steady-state voltammograms of the new 3×3 array and the previous 2×2 array recorded with the potentiostat in Tyrode buffer solution and 15 μM adrenaline. A scan-rate of 50 mV/s was used.

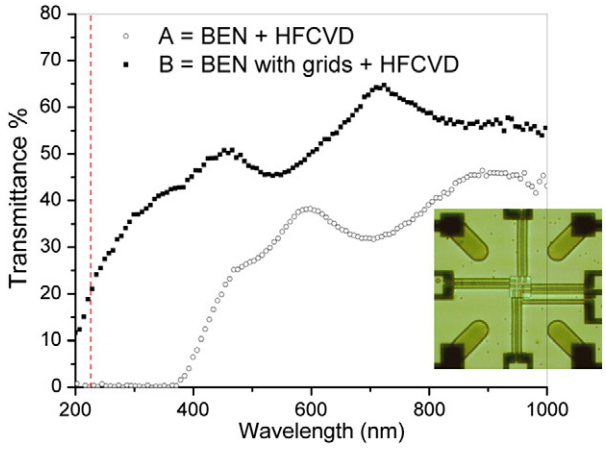

Fig. 7. Transmittance curves of B-doped NCD thin films nucleated with a BEN process: curve A (filled dots) refers to a ~270 nm intrinsic HFCVD NCD + 50 nm B-doped Plasma NCD film realized with thick BEN interlayers. Curve B (empty dots) depicts otherwise the transmittance of a ~200 nm intrinsic + 300 nm B-doped HFCVD NCD film nucleated with thinner interlayers and Pt bias grids. Inset: transmission microscope image of the final NCD high density MEA.

BEN. In this case, extremely thin nucleation interlayers were used together with Pt grids to providing the needed bias for the nucleation process: the transmittance in the UV-range is larger due to a partial consumption of the interlayers during the BEN process itself. The comparison between curves A and B shows that with BEN is possible to achieve the same transparency properties obtained with other seeding techniques [39,40]. We can conclude that not only the average transmittance is higher, but also the full exploitation of wavelengths down to the diamond bandgap limit is then fulfilled (see Fig. 7).

4. Conclusion

We fabricated a new 3×3 high density MEA out of boron-doped NCD on sapphire for amperometric detection with micrometer spatial resolution. The outstanding properties of boron-doped NCD micro-electrodes in electrochemical environment, combined with the promising on-sapphire technology and the possibility to achieve spatially resolved detection in the μm-scale, open the way to electrochemical applications in many fields of research. We characterized the new device in saline and physiological buffer solutions and in the presence of oxidizing species, like adrenaline and ferrocyanide. These characterizations provided evidence of the excellent diamond electrochemical properties and demonstrated the suitability of the NCD 3×3 MEA for high sensitivity electrochemical applications in electrophysiology. In this regard, we compared the amperometric response of the new nine channels device with that of our previous quadrupole prototype, successfully employed for the detection of bursts of adrenaline released by living mouse chromaffin cells. The adrenaline oxidation current density of the new 3×3 array increased by a factor 2 with respect to the 2×2 array, while maintaining a comparable background current.

By combining NCD electrodes with GaN FET electronics, the new concept of NCD MEA on sapphire can approach the integration complexity of CMOS MEAs based on silicon technology. The present study suggests also the suitability of these integrated technologies for low-wavelength transparency applications, which could be coupled to the electrochemical detection.

Acknowledgments

This work was supported by the “Baden-Württemberg Stiftung”, the AIT/DAAD Vigoni program and Regione Piemonte. The authors want to thank A. Trasser and C. Steinmann for their contribution to this work.

References

[1] Y. Zhou, J. Zhi, Talanta 79 (2009) 1189.
[2] M. Panizza, G. Cerisola, Electrochim. Acta 51 (2005) 191.
[3] P.L. Hagans, P.M. Natishan, B.R. Stoner, W.E. O'Grady, J. Electrochem. Soc. 148 (2001) E298.
[4] C. Terashima, T.N. Rao, B.V. Sarada, A. Fujishima, Chem. Lett. 32 (2003) 136.
[5] S. Szunerits, R. Boukherroub, J. Solid State Electrochem. 12 (2008) 1205.
[6] J.B. Miller, D.W. Brown, Langmuir 12 (1996) 5809.
[7] P. Ariano, P. Baldelli, E. Carbone, A. Gilardino, A. Lo Giudice, D. Lovisolo, C. Manfredotti, M. Novara, H. Sternchulte, E. Vittone, Diamond Relat. Mater. 14 (2005) 669.
[8] S. Wenmackers, V. Vermeeren, M. vandeVen, M. Ameloot, N. Bijnens, K. Haenen, L. Michiels, P. Wagner, Phys. Status Solidi A 206 (2009) 391.
[9] R. Pamesham, M.F. Rose, Diamond Relat. Mater. 6 (1997) 17.
[10] M.E. Thomas, W.J. Tropf, A. Szpak, Diamond Films Technol. 5 (1995) 159.
[11] N.S. Lawrence, M. Pagels, A. Meredith, T.G.J. Jones, C.E. Hall, C.S.J. Pickles, H.P. Godfried, C.E. Banks, R.G. Compton, L. Jiang, Talanta 69 (2009) 829.
[12] S. Raina, W.P. Kang, J.L. Davidson, Diamond Relat. Mater. 19 (2010) 256.
[13] M. Bonnauron, S. Saada, L. Rousseau, G. Lissorgues, C. Mer, P. Bergonzo, Diamond Relat. Mater. 17 (2008) 1399.
[14] K.L. Soh, W.P. Kang, J.L. Davidson, Y.M. Wong, D.E. Cliffel, G.M. Swain, Diamond Relat. Mater. 17 (2008) 900.
[15] 15M. You, F. Chau-Nan Hong, Y. Jeng, S.M. HuangM, Diamond Relat. Mater. 18 (2009) 155.
[16] P.T. Joseph, N. Tai, Y. Chen, H. Cheng, I. Lin, Diamond Relat. Mater. 17 (2008) 476.
[17] M. Daenen, O.A. Williams, J.D'. Haen, K. Haenen, M. Nesládek, Phys. Status Solidi 203 (2006) 3005.
[18] O. Auciello, V. Sumant, Diamond Relat. Mater. 19 (2009) 699.
[19] M. Bonnauron, S. Saada, C. Mer, C. Gesset, O.A. Williams, L. Rousseau, E. Scorsone, P. Mailley, M. Nesladek, J.-C. Arnault, P. Bergonzo, Phys. Status Solidi A 9 (2008) 205.
[20] Z. Gao, V. Carabelli, E. Carbone, E. Colombo, F. Demaria, M. Dipalo, S. Gosso, Ch. Manfredotti, A. Pasquarelli, S. Rossi, Y. Xu, E. Vittone, E. Kohn, Diamond Relat. Mater. 19 (2010) 1021.
[21] A. Marcantoni, V. Carabelli, D.H. Vandael, V. Comunanza, E. Carbone, Pflügers Arch. 457 (2009) 1093.
[22] Z. Gao, V. Carabelli, E. Carbone, E. Colombo, M. Dipalo, C. Manfredotti, A. Pasquarelli, M. Feneberg, K. Thonke, E. Vittone, E. Kohn, Journal of Micro-Nano Mechatronics 6 (2011) 33.
[23] V. Carabelli, S. Gosso, A. Marcantoni, A. Pasquarelli, Y. Xu, E. Colombo, Z. Gao, J. Scharpf, E. Kohn, E. Carbone, Biosens. Bioelectron. 26 (2010) 92.
[24] A. Lambacher, V. Vitzthum, G. Zeck, P. Fromherz, Biophys. J. 96 (2009) 478a.
[25] http://www.multichannelsystems.com/
[26] L. Berdondini, P. Massobrio, M. Chiappalone, M. Tedesco, K. Imfeld, A. Maccione, M. Gandolfo, M. Koudelka-Hep, S. Martinoia, J. Neurosci. Methods 177 (2009) 386.
[27] G. Charvet, L. Rousseau, O. Billoint, S. Gharbi, J. Rostaing, S. Joucla, M. Trevisiol, A. Bourgerette, P. Chauvet, C. Moulin, F. Goy, B. Mercier, M. Colin, S. Spirkovitch, H. Fanet, P. Meyrand, R. Guillemaud, B. Yvert, Biosens. Bioelectron. 25 (2010) 1889.
[28] P.J. Koester, C. Tautorat, H. Beikirch, J. Gimsa, W. Baumann, Biosens. Bioelectron. 26 (2010) 1731.
[29] M. Dipalo, Z. Gao, J. Scharpf, C. Pietzka, M. Alomari, F. Medjdoub, J.-F. Carlin, N. Grandjean, S. Delage, E. Kohn, Diamond Relat. Mater. 18 (2009) 88.
[30] Z. Gao, M. Dipalo, A. Pasquarelli, M. Feneberg, K. Thonke, E. Kohn, proceedings of the SBDD XIV 2009, Hasselt (Belgium).
[31] K. Janischowsky, W. Ebert, E. Kohn, Diamond Relat. Mater. 12 (2003) 336.
[32] M. Kunze, A. Vescan, G. Dollinger, A. Bergmaier, E. Kohn, Carbon (1999) 787.
[33] M.I. Montenegro, M.A. Queiros, J.L. Daschbach, Microelectrodes: Theory and Applications, Kluwer Academic Publishers, 1991.
[34] K. Stulik, C. Amatore, K. Holub, V. Marecek, W. Kuntner, Pure Appl. Chem. 72 (2000) 1483.
[35] P. Hernandez, I. Sanchez, F. Paton, L. Hernandez, Talanta 46 (1998) 985.
[36] C. Amatore, Y. Bouret, L. Midrier, Chem. Eur. J. 5 (1999) 2151.
[37] J.E. Baur, R.M. Wightman, J. Electroanal. Chem. 305 (1991) 73.
[38] T.J. Davies, R.G. Compton, J. Electroanal. Chem. 585 (2005) 63.
[39] P.T. Joseph, N. Tai, Y. Chen, H. Cheng, I. Lin, Diamond Relat. Mater. 17 (2008) 476.
[40] M. You, F. Hong, Y. Jeng, S. Huang, Diamond Relat. Mater. 18 (2009) 155.